ANNALS of Clinical and Translational Neurology
Open Access
AMERICAN NEUROLOGICAL ASSOCIATION

RESEARCH ARTICLE

Resting-state fMRI functional connectome of *C9orf72* mutation status

Mario Stanziano[1,2,*], Davide Fedeli[1,*], Umberto Manera[2,3], Stefania Ferraro[1,4], Jean P. Medina Carrion[1], Sara Palermo[1], Paola Sciortino[5], Maurizio Cogoni[5], Federica Agosta[6,7,8], Silvia Basaia[6], Massimo Filippi[6,7,8,9,10], Marina Grisoli[1], Maria C. Valentini[5], Filippo De Mattei[2,3], Antonio Canosa[2,3], Andrea Calvo[2,3], Maria G. Bruzzone[1], Adriano Chiò[2,3,11], Anna Nigri[1] & Cristina Moglia[2,3]

[1]Neuroradiology Unit, Foundation IRCCS Neurological Institute Carlo Besta, Milan, Italy
[2]ALS Centre, "Rita Levi Montalcini" Department of Neuroscience, University of Turin, Turin, Italy
[3]Azienda Ospedaliero-Universitaria Città della Salute e della Scienza di Torino, SC Neurologia 1U, Turin, Italy
[4]MOE Key Laboratory for Neuroinformation, School of Life Science and Technology, University of Electronic Science and Technology of China, Chengdu, China
[5]Neuroradiology Unit, CTO Hospital, AOU Città della Salute e della Scienza di Torino, Turin, Italy
[6]Neuroimaging Research Unit, Division of Neuroscience, IRCCS San Raffaele Scientific Institute, Milan, Italy
[7]Neurology Unit, IRCCS San Raffaele Scientific Institute, Milan, Italy
[8]Vita-Salute San Raffaele University, Milan, Italy
[9]Neurorehabilitation Unit, IRCCS San Raffaele Scientific Institute, Milan, Italy
[10]Neurophysiology Service, IRCCS San Raffaele Scientific Institute, Milan, Italy
[11]Institute of Cognitive Sciences and Technologies, National Council of Research, Rome, Italy

Correspondence
Anna Nigri, Neuroradiology Unit, Foundation IRCCS Neurological Institute Carlo Besta, Via Celoria 11, Milan, Italy. Tel: +390223942595; Fax: +39 0270638217; E-mail: anna.nigri@istituto-besta.it

Funding Information
This work was in part supported by the Italian Ministry of Health (Ministero della Salute, Ricerca Sanitaria Finalizzata and Giovani ricercatori, grant RF-2016-02362405, GR-2019-12371291, RRC), the European Commission's Health Seventh Framework Programme (FP7/2007-2013 under grant agreement 259867), the Italian Ministry of Education, University and Research (Progetti di Ricerca di Rilevante Interesse Nazionale, PRIN, grant 2017SNW5MB), the Joint Programme – Neurodegenerative Disease Research (ALS-Care, Strength and Brain-Mend projects), granted by Italian Ministry of Education, University and Research. This study was performed under the Department of Excellence grant of the Italian Ministry of Education, University and Research to the 'Rita Levi Montalcini' Department of Neuroscience, University of Torino, Italy.

Received: 7 July 2023; Revised: 15 November 2023; Accepted: 16 December 2023

Abstract

Objective: The resting-state functional connectome has not been extensively investigated in amyotrophic lateral sclerosis (ALS) spectrum disease, in particular in relationship with patients' genetic status. **Methods**: Here we studied the network-to-network connectivity of 19 ALS patients carrying the *C9orf72* hexanucleotide repeat expansion (*C9orf72+*), 19 ALS patients not affected by *C9orf72* mutation (*C9orf72−*), and 19 ALS-mimic patients (*ALSm*) well-matched for demographic and clinical variables. **Results**: When compared with ALSm, we observed greater connectivity of the default mode and frontoparietal networks with the visual network for *C9orf72+* patients ($P = 0.001$). Moreover, the whole-connectome showed greater node degree ($P < 0.001$), while sensorimotor cortices resulted isolated in *C9orf72+*. **Interpretation**: Our results suggest a crucial involvement of extra-motor functions in ALS spectrum disease. In particular, alterations of the visual cortex may have a pathogenic role in *C9orf72-related* ALS. The prominent feature of these patients would be increased visual system connectivity with the networks responsible of the functional balance between internal and external attention.

***Annals of Clinical and Translational Neurology* 2024; 11(3): 686–697**

doi: 10.1002/acn3.51989

*These authors equally contributed to the paper.

Introduction

Amyotrophic lateral sclerosis (ASL) is a neurodegenerative disorder that affects motor neurons in the brain and spinal cord.[1,2] Alongside progressive muscular atrophy and motor symptoms, 15–20% of ALS patients present non-motor symptoms, behavioral changes, and severe cognitive deficits within the ALS—frontotemporal dementia (FTD) clinical spectrum. Growing evidence has linked ALS with a set of genetic mutations.[3] In particular, the intronic hexanucleotide G_4C_2 expansion in the chromosome 9 open reading frame 72 (*C9orf72*) is the major genetic cause of ALS and FTD and it is associated with more severe forms of ALS.[4,5] This mutation has been observed in 20–40% of familial and 3–8% of sporadic ALS cases.[6,7] The disease onset is earlier in mutation carriers (*C9orf72*+), typically characterized by with bulbar signs, cognitive symptoms, and faster disease progression that leads to a shorter survival.[8–10] Structural imaging analyses have also revealed widespread extra-motor pathology in addition to motor cortex damage in *C9orf72*+ patients.[11–13] Mutation carriers show gray matter volume loss and cortical thinning in the primary motor cortex, extending to prefrontal, occipitotemporal, and parietal areas,[11,13–15] alongside significant thalamic atrophy.[11,12,14,16] Despite this extensive corpus of knowledge, functional network alterations in ALS according to genetic mutations are still insufficiently investigated. Only few resting-state functional magnetic resonance imaging (rs-fMRI) studies have been performed on this topic and the abnormal connectivity organization in *C9orf72*+ ALS patients is still only marginally understood.[11,17–20] This literature gap is particularly striking when considering that functional connectivity alterations at rest have been suggested to potentially represent the earliest detectable brain abnormality in carriers of ALS-causing gene mutations.[17,21] Previous studies have reported patterns of increased/altered connectivity at rest associated with *C9orf72* mutation. When compared with ALS sporadic cases, *C9orf72*+ patients showed increased connectivity within the visual, anterior default mode, and right dorsal attention networks,[11,19] and diminished connectivity within salience, sensorimotor, posterior default mode, and pulvinar/thalamic-seeded networks.[11,17–19] These connectivity alterations allegedly emerge during development and worsen after disease onset.[18,22] When compared to healthy participants, *C9orf72*+ patients have been reported to show reduced posterior and subcortical connectivity,[20] and decreased meta-states changes[23] (i.e., reduced dynamic changes in brain connectivity patterns). However, the relationship between intrinsic connectivity networks remains unclear and this vast range of alterations does not allow for a systematic understanding of the impact of *C9orf72* mutation on the overall brain's functional organization.

On these grounds, it seems crucial to develop a better understanding of the neurofunctional differences between mutation carriers and non-mutation carriers. In this study, we used rs-fMRI to compare a group of ALS patients carrying the *C9orf72* hexanucleotide repeat expansion (*C9orf72*+), with a group of well-matched patients not affected by the gene mutation (*C9orf72*−), and a control group of ALS mimics patients[24] (*ALSm*). Participants were carefully matched for disease severity, as previuously described,[25] to describe the genotype signature controlling for clinical phenotypes. In this study, we used a functional network connectivity[26] (FNC) approach to investigate the impact of *C9orf72* mutation on both intra- and inter-network connectivity. Based on previous evidence of alterations within single connectivity networks, we expect *C9orf72* mutation to significantly affect the brain's between-networks organization.

If proven significant, the relationship between inter-network connectivity and *C9orf72* mutations in ALS would allow a broader understanding of *C9orf72*-based alterations and potentially represent an early-detectable biomarker in asymptomatic and presymptomatic carriers.

Materials and Methods

Participants

Thirty-eight ($N = 38$) patients diagnosed with ALS (EI Escorial Revised Criteria[27]), and 19 ($N = 19$) *ALSm* patients took part to the study. Comorbidity of severe neurological or psychiatric conditions as well as causes of focal or diffuse brain damage, including lacunae, and extensive cerebrovascular disorders at routine MRI were considered as exclusion criteria. Nineteen ALS patients carried the *C9orf72* hexanucleotide repeat expansion (*C9orf72*+), while 19 ALS patients were not affected by the pathological *C9orf72* expansion (*C9orf72*−). The group of *ALSm*

patients included in this study did not have primary neurodegenerative diseases but rather clinical conditions with features resembling those of ALS: cervical spondylotic myelopathy ($N = 3$), myasthenia gravis ($N = 9$), monomelic amyotrophy (Hirayama) ($N = 1$), and peripheric motor neuropathy ($N = 6$). All ALSm patients were initially recruited as suspected or possible ALS cases and were later diagnosed as mimics. *ALSm*, *C9orf72+*, and *C9orf72−* participants were carefully matched for age and sex assigned at birth using a one-by-one pairing technique. *C9orf72+* and *C9orf72−* patients were additionally matched for ALSFRS-total score and disease duration. Number of body regions involved was assessed using King's staging system[28] (KSS). All included patients had no mutation in *SOD1*, *TARDBP*, and *FUS* genes. Demographic and clinical data are reported in Table 1.

The study was carried out in accordance with the Declaration of Helsinki; all clinical data were collected and analyzed under the local ethics committee approval (Azienda Ospedaliero-Universitaria Città della Salute e della Scienza di Torino, SC Neurologia 1U, Turin, Italy). All participants gave their written consent.

MRI acquisition

Magnetic resonance imaging acquisition was performed with a 1.5 Tesla General Electric Signa HD-XT scanner (General Electric, Milwaukee, WI, USA) equipped with an eight channels *8HRBrain* head coil, at the unit of Neuroradiology Unit, CTO Hospital, AOU Città della Salute e della Scienza di Torino, Italy. For each participant a T1-weighted anatomical image was acquired with the following parameters: repetition time [TR] = 11.85 ms, echo time [TE] = 4.9 ms, flip angle [FA] = 12°, field of view [FOV] = 240 mm, number of axial slices = 120, voxel size = 0.47 × 0.47 × 1 mm^3, and whole-brain coverage. rs-fMRI scans were acquired with a fast speed Echo Planar Imaging sequence with the following parameters TE = 50 ms; TR = 2250 ms; FA = 90°; number of volumes = 585; FOV = 210; 25 axial slices per volume;

Table 1. Demographic and clinical data.

	C9orf72+ ($N = 19$)	*C9orf72−* ($N = 19$)	*ALSm* ($N = 19$)	P^a
Male/female ratio	10/9	10/9	10/9	1
Bulbar/spinal onset	13/6	11/8	–	0.68
Cognitive classification	*n*	*n*	–	0.36
Normal cognition	7	11	–	
ALSbi	1	2	–	
ALSci	2	1	–	
ALScbi	1	0	–	
ALS-FTD	4	1	–	
Unknown	4	4	–	
KSS (number of body regions involved)	*n*	*n*	–	0.58
KSS 1	9	7	–	
KSS 2	5	8	–	
KSS 3	4	2	–	
KSS 4	1	2	–	
	Median (IQR)	Median (IQR)	Median (IQR)	P^b
Age (years)	55.50 (51.15–69.70)	59.50 (53.45–66.05)	60.00 (53.00–69.00)	0.99
ALSFRS-R score	43.00 (38.50–45.00)	43.00 (37.50–45.00)	–	0.95
Disease duration (months)	11.0 (8.00–14.50)	11.0 (9.00–13.50)	–	0.94
Overall survival (years)	2.57 (2.19–3.17)	2.70 (2.13–3.40) (4 alive)	–	0.91
Disease progression (ΔALSFRS-R)	0.53 (0.28–0.78)	0.56 (0.27–0.91)	–	0.67

KSS, King's staging score system; IQR, interquartile range; ALSFRS-R, Revised Amyotrophic Lateral Sclerosis Functional Rating Scale.
[a]Indicates results for chi-squared test between *C9orf72+*, *C9orf72−*, and *ALSm*.
[b]Indicates results for two-sample independent *t*-tests between *C9orf72+* and *C9orf72−*, or one-way ANOVA tests between *C9orf72+*, *C9orf72−*, and *ALSm*.

slice thickness = 4; interslice gap = 1 mm; voxel size = 3.28 × 3.28 × 5 mm^3; phase encoding direction = anterior/posterior; the cerebellum was only partially included in the volume coverage. Participants were asked to keep their eyes closed during the rs-fMRI acquisition.

Statistical analyses

Demographical analyses

Analyses were performed with SciPy[29] running on Python3. Parametric tests were performed for all demographic and clinical variables, except for those not normally distributed (according to the Kolmogorov–Smirnov test). Differences in age (years) between all three groups were tested with Kruskal–Wallis ANOVA. Group differences in sex assigned at birth distribution were tested with chi-squared statistics. Differences in clinical variables (i.e., bulbar vs. spinal onset, ALSFRS-R score, disease duration in months, survival in years, disease progression, and number of body regions involved) were tested between *C9orf72+* and *C9orf72−* with independent sample *t*-tests and Mann–Whitney *U* tests. All results were considered as significant at $P \leq 0.05$ and corrected for multiple comparisons.

Preprocessing

T1-weighted anatomical images were segmented with FreeSurfer (v6.0.0, http://surfer.nmr.mgh.harvard.edu/).[30] The estimated total intracranial volume (TIV), representing the sum of total gray matter, white matter (WM), and cerebrospinal fluid volume (CSF), was extracted for each participant using the same tool. Kolmogorov–Smirnov test was performed to assess the normal distribution of each variable. Group differences in TIV were computed using a one-way ANOVA to determine the overall atrophy degree in patients' subgroups.

The CONN toolbox[31] (version 20.b; MATLAB 9.14) implemented in SPM12 was used to perform neuroimaging data preprocessing and resting-state functional connectivity analyses. CONN's "default_MNI" preprocessing pipeline was used. The following processing steps were performed: realignment to the first functional image and unwarping, slice-timing correction (slice order = interleaved, bottom-up); outlier identification with the artifact rejection toolbox (ART) (ART thresholds: framewise displacement >1.1 mm; global BOLD signal changes >5 SD); direct segmentation in gray matter, WM, and CSF tissue classes; registration and normalization of functional and anatomical data into standard Montreal Neurological Institute (MNI) space[32]; functional data resampling to 2 mm isotropic voxels, and anatomical data resampling to 1 mm isotropic voxels; smoothing with a full-width at half-maximum 6 × 6 × 6 mm^3 Gaussian kernel. Data denoising was performed with the anatomical component-based noise correction (aCompCor) to extract noise signal from white matter and CSF components on a voxel-by-voxel level.[33,34] For each participant, realignment parameters, outlier volumes scrubbing parameters, physiological noise components obtained from mean WM and CSF maps, and "effect of rest" (initial magnetization transient effects) were entered as nuisance covariates in the first-level analysis.[35] Subsequently, a 0.008- to 0.1-Hz bandpass filter was applied to the time-series to remove low-frequency drifts and high-frequency noise.

The quality of structural and functional images was assessed and visually inspected using both the quality assessment (QA) tool implemented in CONN's default, and the BIDS-compliant software MRIQC.[36] No participant was excluded because of excessive motion, noise, or other MRI artifacts.

ROI-to-ROI resting-state functional connectivity

A region of interest-to-region of interest (ROI-to-ROI) approach was adopted for the first-level analyses. For each participant, a connectivity matrix including 26 ROIs of the following rs-fMRI networks, as implemented in CONN's default atlas, was computed. Default mode network (medial prefrontal cortex, left lateral parietal region, right lateral parietal region, posterior cingulate cortex), sensorimotor network (left lateral region, right lateral region, superior region), visual network (medial region, occipital region, left lateral region, right lateral region), salience network (anterior cingulate cortex, left anterior insula, right anterior insula, left rostral prefrontal cortex, right rostral prefrontal cortex, left supramarginal gyrus, right supramarginal gyrus), dorsal attention network (left frontal eye field, right frontal eye field, left intraparietal sulcus, right intraparietal sulcus), and frontoparietal network (left lateral prefrontal cortex, right lateral prefrontal cortex, left posterior parietal cortex, right posterior parietal cortex). For each ROI of each rs-fMRI network, Pearson's correlation coefficients were computed between the signal time-series of that ROI and all the other 25 ROIs. Correlation coefficients were then converted to *Z* scores with the R-to-Z Fisher transform and a 26 × 26 whole-connectome matrix was generated for each subject. Connectome matrices were entered into the second-level general linear model to compare the functional connectivity network profiles of patients' subgroups with directional contrasts (i.e., *C9orf72+* vs. *ALSm*, *C9orf72−* vs. *ALSm*, and *C9orf72+* vs. *C9orf72−*). Age, sex assigned at birth, and TIV were included as nuisance covariates.[37–39] The functional

network connectivity (FNC) method implemented in CONN was adopted to perform cluster-level inferences on the rs-fMRI networks of ROIs.[26,35] Briefly, FNC first identifies sets of related ROIs with a data-driven hierarchical clustering procedure. The entire set of connections between all pairs of ROIs is then analyzed using a multivariate parametric general linear model analysis. To select only highly significant pairs of sets of connections the cluster-level *P*-false-discovery rate (FDR)-corrected for multiple comparisons was set at <0.05. To identify only the most robust individual connections of the significant sets the connection-level post hoc uncorrected *P* was set at <0.05. Cluster-level and connection-level significance thresholds were kept at CONN 20b's default settings.

Correlational analyses were performed to determine the impact of disease duration and ALS progression on brain connectivity. For each between-group second level significant comparison, the mean connectivity of the resulting matrix was computed for *C9orf72*+ and *C9orf72*− and correlated with disease duration and King's staging system scores. Moreover, to assess whether variations in network connectivity could be observed across different KSS stages, comparisons between *C9orf72*+ and *C9orf72*− groups were also performed restricting the analysis to stages with at least five participants per group. Finally, as both male sex assigned at birth and spinal onset have been described as factors negatively impacting prognosis in *C9orf72*+ patients,[40] additional comparisons were performed (i.e., male *C9orf72*+ patients vs. female *C9orf72*+ patients; bulbar onset *C9orf72*+ patients vs. spinal onset *C9orf72*+ patients).

Graph theory metrics

In graph theory, the brain's functional organization can be modeled as a complex system of interacting elements (graph) with nodes (ROIs) connected by edges (connections).[41,42] Each participant-specific 26 × 26 ROI-to-ROI connectivity matrix was thresholded at a cost value of $k = 0.3$ as small-world properties were observed at this threshold (as recommended by CONN's guidelines[31]). Accordingly with CONN's default options, single subjects' negative functional connectivity values were disregarded in these analyses. The following graph theory metrics as implemented in CONN were extracted from each participant's whole 26 × 26 ROI-to-ROI connectome: node degree (i.e., the number of connections of each node), global efficiency at a node (i.e., the average of the inverse minimum number of edges between each node and all other nodes in the network, representing a measure of the node's centrality within a network), local efficiency at a node (i.e., the extent of the integration of a sub-graph consisting of only the nodes surrounding a certain node, representing an index of local integration or coherence), and betweenness centrality (i.e., an alternative measure of node centrality representing the proportion of times that a node is part of a shortest path between any two pairs of nodes within a graph).[42] Graph theory metrics were compared between each group with CONN with the same covariates used in the previous for ROI-to-ROI connectivity analyses. All results were corrected with a $P < 0.05$ FDR correction for multiple comparisons.

As the adoption of matrix node thresholds for performing graph analyses can potentially hide small effects, additional analyses were performed with *K* cost threshold set at 0.1; 0.3 (our default); 0.5; 0.7; 0.9, respectively indicating that the analyses were performed only with the top 10%, 30%, 50%, 70%, and 90% of the connectome edges.

Results

Demographical analyses

No significant difference in age between the three groups was found ($H = 0.03$, $P = 0.98$). No significant difference in ALSFRS-R at the time of MRI ($T = 0.06$, $P = 0.95$) and disease duration from the onset ($U = 169.5$, $P = 0.76$) was found between *C9orf72*+ and *C9orf72*− patients. When comparing TIV among each group, no significant difference emerged ($F = 0.55$, $P = 0.58$).

ROI-to-ROI resting-state functional connectivity

The comparison between *C9orf72*− and *ALSm* patients did not reveal significant differences. Similarly, no significant difference in network connectivity between *C9orf72*+ and *C9orf72*− patients was found.

C9orf72+ patients when compared to *ALSm* revealed significant differences in the connectivity of one set of networks ($F(2, 50) = 11.14$, *P*-FDR-corrected for multiple comparisons = 0.001, $\eta^2 \approx 0.92$; 95% CI = 0.85–0.96). In particular, *C9orf72*+ patients relative to *ALSm* exhibited increased connectivity between the default mode network (bilateral lateral parietal components, medial prefrontal cortex, posterior cingulate cortex) and the visual network (medial, occipital, and bilateral lateral components), and between the frontoparietal network (bilateral posterior parietal cortex, bilateral prefrontal cortex) and the visual network (medial, occipital, and bilateral lateral components). Results are reported in Table 2; and Fig. 1A.

No significant correlations between the mean connectivity of significant networks and disease duration, and KSS score were identified. No significant difference was observed when grouping patients by KSS stages. No significant difference associated with male sex assigned at birth or bulbar onset were observed in the *C9orf72*+ group.

Table 2. ROI-to-ROI resting-state functional connectivity results.

Cluster	*F*-value	*P*-FDR
Whole network	11.41	<0.001

Region 1	MNI *xyz* coordinates	Region 2	MNI *xyz* coordinates	*T*-value	*P*-unc
Visual lateral (L)	−37, −79, 10	Default mode LP (L)	−39, −77, 33	4.01	<0.001
Visual lateral (R)	38, −72, 13	Frontoparietal LPFC (R)	41, 38, 30	3.82	<0.001
Visual lateral (R)	38, −72, 13	Default mode LP (R)	47, −67, 29	3.78	<0.001
Visual lateral (L)	−37, −79, 10	Default mode LP (R)	47, −67, 29	3.66	<0.001
Visual lateral (R)	38, −72, 13	Frontoparietal PPC (L)	−46, −58, 49	3.44	0.001
Visual lateral (R)	38, −72, 13	Default mode LP (L)	−39, −77, 33	3.43	0.001
Visual lateral (R)	38, −72, 13	Default mode PCC	1, −61, 38	3.28	0.002
Visual lateral (R)	38, −72, 13	Frontoparietal LPFC (L)	−43, 33, 28	3.24	0.002
Visual lateral (L)	−37, −79, 10	Frontoparietal LPFC (R)	41, 38, 30	3.14	0.003
Visual occipital	0, −93, −4	Default mode LP (R)	47, −67, 29	3.17	0.003
Visual occipital	0, −93, -4	Default mode LP (L)	−39, −77, 33	3.17	0.003
Visual lateral (L)	−37, −79, 10	Frontoparietal PPC (R)	52, −52, 45	2.79	0.007
Visual lateral (L)	−37, −79, 10	Frontoparietal LPFC (L)	−43, 33, 28	2.75	0.008
Visual lateral (L)	−37, −79, 10	Default mode PCC	1, −61, 38	2.7	0.009
Visual medial	2, −79, 12	Default mode LP (R)	47, −67, 29	3.38	0.001
Visual medial	2, −79, 12	Default mode LP (L)	−39, −77, 33	3.13	0.003
Visual lateral (R)	38, −72, 13	Frontoparietal PPC (R)	52, −52, 45	2.6	0.012
Visual lateral (L)	−37, −79, 10	Frontoparietal PPC (L)	−46, −58, 49	2.46	0.017
Visual lateral (L)	−37, −79, 10	Default mode MPFC	1, 55, −3	2.23	0.03
Visual medial	2, −79, 12	Frontoparietal LPFC (R)	41, 38, 30	2.6	0.012
Visual medial	2, −79, 12	Frontoparietal LPFC (L)	−43, 33, 28	2.18	0.034
Visual medial	2, −79, 12	Default mode MPFC	1, 55, −3	2.15	0.036
Visual occipital	0, −93, −4	Frontoparietal PPC (R)	52, −52, 45	2.03	0.047

Significance threshold is set at *P*-false-discovery rate (FDR)-corrected <0.05 (cluster level) and at *P*-uncorrected <0.05 (connection level). L, left; R, right.

Graph theory metrics

When comparing *C9orf72+* with *ALSm*, graph theory analyses showed a significant enhancement in the node degree of the whole connectome in the former (i.e., the whole system of interconnected networks; $T(51) = 4.65$, *P*-unc < 0.001, $d = 0.65$, 95% CI = 0.22 to 1.08). Conversely, the bilateral lateral nodes of sensorimotor network showed decreased node degree (left node: $T(51) = -3.78$, *P*-FDR = 0.011, $d = -0.53$, 95% CI = −1.06 to 0; right node: $T(51) = -3.19$, *P*-FDR = 0.032; $d = -0.45$, 95% CI = −1.08 to 0.18) and decreased global efficiency at node (left node: $T(51) = -3.78$, *P*-FDR = .009, $d = -0.53$, 95% CI = −1.06, −0; right node: $T(51) = -3.58$, *P*-FDR = 0.009; $d = -0.5$, 95% CI = −1.06 to 0.06) in *C9orf72+* patients.

No significant difference was found when considering local efficiency and betweenness centrality, and when comparing *C9orf72+* with *C9orf72−* and *C9orf72−* with *ALSm* patients. Whole-connectome main effects for each group are reported in Figure 1B.

Analyses performed with *K* cost threshold values ranging from 0.1 to 0.9 are reported in the Table S1 section.

Discussion

The relationship between brain functional connectivity at rest and the gene mutation status in ALS is not fully understood. This lack of consistency may depend, at least in part, on adequate patients-controls matching and methodological choices in data processing. In particular, most of the aforementioned studies adopted an independent component analysis-based approach to explore connectivity changes within—and not between—isolated networks. Due to the brain's complex and interconnected nature, neurological disorders are known to disrupt communication between multiple interdependent large-scale functional connectivity networks.[41,43–45] In this study, we tested inter- and intra-network connectivity between *C9orf72* mutation carriers, noncarriers, and ALS-mimic patients. Two main results were obtained when comparing *C9orf72+* with *ALSm*. Functional Network Connectivity analyses revealed enhanced connectivity of the visual network with both the default mode network and the frontoparietal network. Moreover, graph theoretical metrics revealed increased number of connections within the whole connectome in the

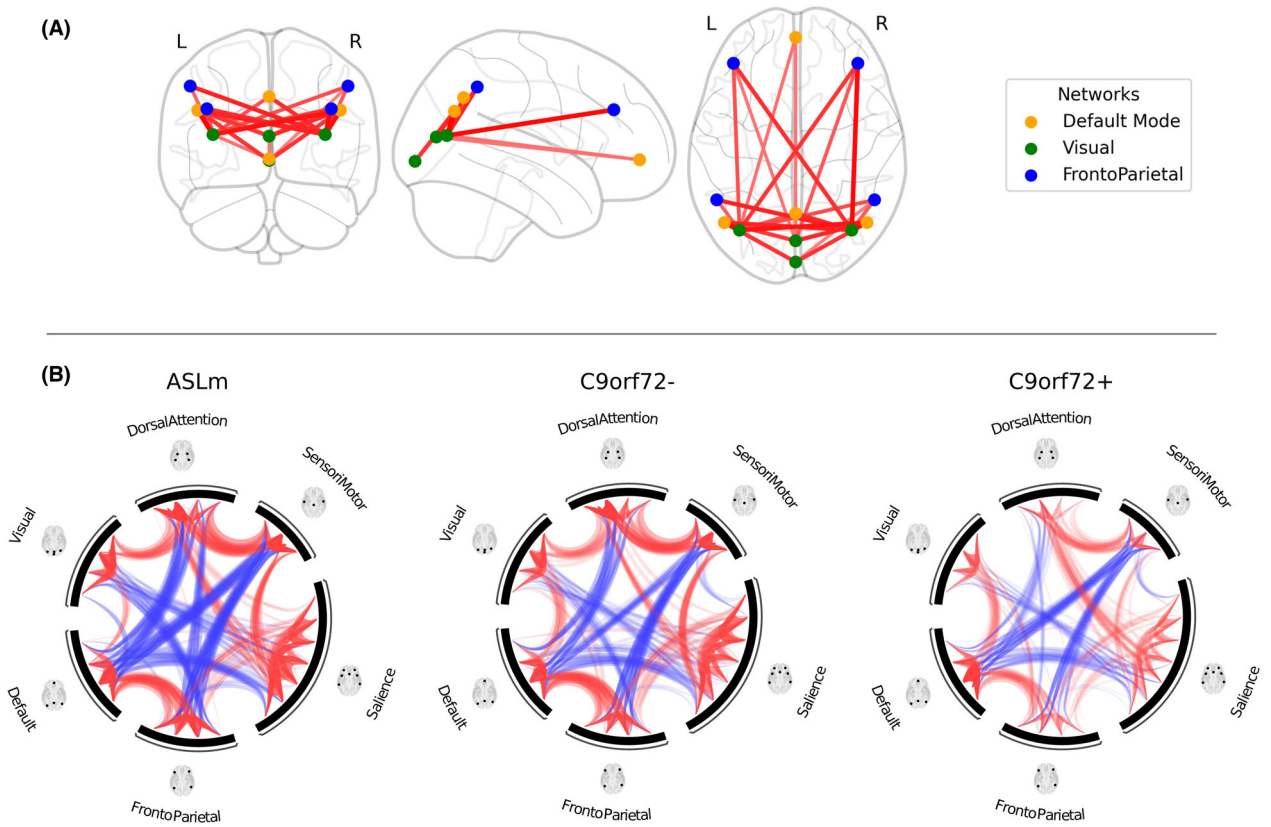

Figure 1. (A) Results from the *C9orf72+ > ALSm* contrast, in the ROI-2-ROI analyses. Results are shown at connection-*P*-uncorrected <0.05, cluster-*P*-FDR-corrected for multiple comparisons <0.05. L = left; R = right. Red color indicates increased ROI-to-ROI connectivity. (B) Resting-state functional connectivity main effects at the whole-connectome level. Results are shown at connection-*P*-uncorrected <0.05, cluster-*P*-FDR-corrected for multiple comparisons <0.05. Red color indicates positive ROI-to-ROI connectivity, blue color indicates negative ROI-to-ROI connectivity.

face of functional segregation of sensorimotor bilateral nodes.

In this study, the visual system resulted more strongly connected with anterior and posterior regions of the default mode network and the frontoparietal network in *C9orf72+* when compared to *ALSm*. Early pathological changes within the occipital cortex accompanied by local functional and structural abnormalities have been reported in *C9orf72+* patients.[46–48] Agosta and colleagues[11] showed enhanced visual functional connectivity in *C9orf72+* patients in the presence of occipital cortical thinning and decreased inferior frontooccipital fasciculus microstructural integrity. Moreover, Premi and colleagues[23] recently reported a *C9orf72* mutation-driven association between pathological brain connectivity and processing speed in a visual search task (TMT-A) that might support a negative impact of gene mutation on visuospatial functions.

On the other hand, alterations in both default mode and frontoparietal networks have been reported in mutation carriers. The default mode network consists of a group of interconnected brain regions whose activity increases while at rest and during "inactive" states (e.g., self-referential processing and mind wandering), and decreases when the brain is engaged in attention-demanding and goal-directed tasks.[49,50] Conversely, the frontoparietal network is part of the "central executive network" whose activity is typically associated with directing attention to perform intentional goal-driven behavior and exert adaptive cognitive control.[51,52] In *C9orf72+* patients with respect to sporadic cases and healthy participants, both increased and decreased connectivity within the default mode network have been observed.[17–19] Comparing presymptomatic *C9orf72+* participants with healthy participants, longitudinal trajectories of intra-network homogeneity of the frontoparietal network showed increased connectivity as aging.[22] Moreover, according to the well-known "triple network model," the activity of the default mode network and the frontoparietal network is typically found to be connected and mediated by the salience network, as attention naturally switches from internal to external awareness states and vice-versa.[53]

Alteration of this specific functional organization of information transfer would be impactful on executive functions sustained by the main hubs of these large-scale networks, such as prefrontal, parietal, and cingulate cortices.[54–56] This interpretation is in line with neuropsychological evidence of greater impairment in executive functions, and visual and verbal memory in *C9orf72* mutation carriers when compared with *C9orf72*− patients.[9] The altered visual network connectivity with the default mode and frontoparietal networks in *C9orf72*+ patients is an original finding of this study that needs to be further explored. A potential explanatory interpretation may involve the causal relationship between thalamic degeneration in *C9orf72*+ patients and dysfunctions in brain connectivity at rest. Thalamic alterations have been recurrently reported in mutation carriers, and have been considered a robust morphological signature of *C9orf72* mutation.[14,16,47,57,58] In particular, pulvinar nuclei within the thalamus are a fundamental point of convergence in visual pathways and are involved in visual cognition and visuospatial attention processes. Moreover, pulvinar nuclei are functionally and anatomically connected with the visual network and have topographically organized visual field maps.[59,60] Lee and colleagues[17,18] observed medial pulvinar degeneration associated with disrupted salience network connectivity in *C9orf72*+ presymptomatic patients when compared with healthy controls (see also Premi and colleagues[23]). Our findings may suggest that the visual network in *C9orf72*+ patients, potentially "disanchored" from atrophic pulvinar nuclei, loses its functional specificity and becomes more strongly connected with internal and external attention networks that are typically mediated by the salience network in healthy controls.[53]

Considering graph theoretical metrics, our results revealed that *C9orf72*+ patients are characterized by a connectome with a larger number of connections. This finding is in line with previous accounts of increased resting-state connectivity observed in *C9orf72* mutation carriers[11,19] and it is most probably mirrored at the structural connectivity level.[61] Hyperconnected systems (i.e., enhanced functional connectivity in terms of the number or the strength of connections) have been observed in several neurological and psychiatric disorders, either as a compensatory response to neurological disruption or following the loss of local inhibition.[21,62–64] According to graph theory, network hyperconnectivity generally indicates high-cost information transfer, with redundant connections that are metabolically expensive to maintain and associated with increased vulnerability to pathologies.[42,64,65] In addition to whole-connectome increased number of connections, *C9orf72*+ patients showed isolated sensorimotor cortices when compared with the *ALSm* group. This finding is in line with the known alterations of the sensorimotor cortex integrity and connectivity observed in ALS patients, irrespective of the mutation status.[11,22,66] Our results suggest that functional connectivity at rest in *C9orf72*+ patients is costly and inefficient, with abnormalities in high-cost components such as network hubs and long-distance connections.[65] Within this system, sensorimotor processes would be inadequately integrated. This pathological organization allegedly originates from combined neurodevelopmental factors and neurodegenerative processes that would lead to dysfunctional motor and extra-motor behavior in mutation carriers.

Our results should be considered in light of two main limitations. First, it was not possible to collect imaging data from healthy controls due to the hospital setting in which the data were acquired. Comparing our cohorts of patients with a control group of healthy individuals would have allowed a broader understanding of the neurofunctional impact of *C9orf72* mutation in ALS. Nonetheless, the inclusion of *ALSm* patients did allow us to identify those features that are unique to ALS and the *C9orf72* mutation in particular, irrespective of the common symptomatic manifestations with symptomatic mimics. In addition, the group of *ALSm* patients considered in this study did not have primary neurodegenerative diseases, which could have influenced the comparison. Moreover, the heterogeneous group of clinical conditions within the control group might have contributed to significant variability in *ALSm* connectivity. This limitation is again derived by the inherent difficulties in obtaining closely matched healthy controls within a clinical setting. However, such variability could have partially reduced possible between-group differences. The effect size and confidence intervals of the ROI-to-ROI network connectivity comparison indicate a large between-group effect, with a narrow confidence interval, thus suggesting robust effect only marginally influenced by group variability. Nonetheless, future studies could better address this issue directly by enrolling healthy control subjects. As a second limitation, our analyses did not reveal significant differences between *C9orf72*+ and *C9orf72*− patients. The two samples were accurately matched for age, sex assigned at birth, and disease burden. Of note, the mean disease duration in both cohorts was inferior to 1 year. Group differences between mutation and non-mutation carriers may appear later, as dysfunctional connectivity changes over time with dissimilar disease trajectories.[8,18,22,67] On these grounds, the two groups might have been too similar for large-scale network connectivity differences to emerge significantly at this early stage of pathology. A longitudinal study would be better suited to explore mutation-based differences in the impact of disease trajectories on functional connectivity.

Taken together, our results provide an original overview of the impact of the genetic status on large-scale connectivity networks in ALS, paving the way for future research on gene-based connectomics and gene-targeted therapies. *C9orf72* mutation is associated with a neuroimaging phenotype caused by neurodevelopmental and neurodegenerative processes that induce pathological hyperconnectivity between extra-motor networks in the face of sensorimotor network isolation.

Conclusions

In the present study, we used network neuroscience as a methodological framework to investigate how *C9orf72* hexanucleotide expansion in ALS patients affects the brain's functional connectivity at rest. Our findings highlight the unique role played by *C9orf72* mutation in the pathological neurofunctional profile of ALS patients. In particular, mutation carriers showed abnormal visual network connectivity with internal and external attention networks and a broadly hyperconnected connectome with isolated sensorimotor nodes.

Acknowledgments

Our special thanks also to our colleagues. Special acknowledgment should be expressed to the patients who participated in the study and to all the technicians (Francesco Primo, Roberto Agliata, Lucy Stefanelli, Rosalba Caruana, Nicola Mazzei, Manuela D'Ambrosio, Gianfranco Tagliente, Francesca Stancati) and radiologists (Giovanna Carrara, Lequio Laura, Denegri Federica, Ivan Gomez Pavanello, Fabrizio Venturi) at the Neuroradiology Unit of CTO Hospital (AOU Città della Salute e della Scienza di Torino) who supervised the MRI scans. We thank the GARR consortium for the high-performance infrastructure used for the analyses. Open access funding provided by BIBLIOSAN.

Author Contributions

Dr Nigri had full access to all of the data in the study and took responsibility for the integrity of the data and the accuracy of the data analysis.

Conflict of Interest

Adriano Chiò serves on scientific advisory boards for Mitsubishi Tanabe, Biogen, Roche, Denali Pharma, Cytokinetics, Lilly, Zambon Biotech, and Amylyx Pharmaceuticals and has received a research grant from Biogen. No conflicts of interest are present for the other authors.

Data Availability Statement

Data will be available upon request by interested researchers.

References

1. Brown RH, Al-Chalabi A. Amyotrophic lateral sclerosis. N Engl J Med. 2017;377(2):162-172. doi:10.1056/NEJMra1603471
2. Chiò A, Pagani M, Agosta F, Calvo A, Cistaro A, Filippi M. Neuroimaging in amyotrophic lateral sclerosis: insights into structural and functional changes. Lancet Neurol. 2014;13(12):1228-1240. doi:10.1016/S1474-4422(14)70167-X
3. Lill CM, Abel O, Bertram L, Al-Chalabi A. Keeping up with genetic discoveries in amyotrophic lateral sclerosis: the ALSoD and ALSGene databases. Amyotroph Lateral Scler. 2011;12(4):238-249. doi:10.3109/17482968.2011.584629
4. DeJesus-Hernandez M, Mackenzie IR, Boeve BF, et al. Expanded GGGGCC hexanucleotide repeat in noncoding region of C9ORF72 causes chromosome 9p-linked FTD and ALS. Neuron. 2011;72(2):245-256. doi:10.1016/j.neuron.2011.09.011
5. Renton AE, Majounie E, Waite A, et al. A hexanucleotide repeat expansion in C9ORF72 is the cause of chromosome 9p21-linked ALS-FTD. Neuron. 2011;72(2):257-268. doi:10.1016/j.neuron.2011.09.010
6. Grassano M, Calvo A, Moglia C, et al. Systematic evaluation of genetic mutations in ALS: a population-based study. J Neurol Neurosurg Psychiatry. 2022;93:1190-1193. doi:10.1136/jnnp-2022-328931
7. Marogianni C, Rikos D, Provatas A, et al. The role of C9orf72 in neurodegenerative disorders: a systematic review, an updated meta-analysis, and the creation of an online database. Neurobiol Aging. 2019;84:238.e25-238.e34. doi:10.1016/j.neurobiolaging.2019.04.012
8. Glasmacher SA, Wong C, Pearson IE, Pal S. Survival and prognostic factors in C9orf72 repeat expansion carriers: a systematic review and meta-analysis. JAMA Neurol. 2020;77(3):367-376. doi:10.1001/jamaneurol.2019.3924
9. Iazzolino B, Peotta L, Zucchetti JP, et al. Differential neuropsychological profile of patients with amyotrophic lateral sclerosis with and without C9orf72 mutation. Neurology. 2021;96(1):e141-e152. doi:10.1212/WNL.0000000000011093
10. Van Der Ende EL, Jackson JL, White A, Seelaar H, Van Blitterswijk M, Van Swieten JC. Unravelling the clinical spectrum and the role of repeat length in C9ORF72 repeat expansions. J Neurol Neurosurg Psychiatry. 2021;92(5):502-509. doi:10.1136/jnnp-2020-325377
11. Agosta F, Ferraro PM, Riva N, et al. Structural and functional brain signatures of C9orf72 in motor neuron disease. Neurobiol Aging. 2017;57:206-219. doi:10.1016/j.neurobiolaging.2017.05.024

12. Li Hi Shing S, McKenna MC, Siah WF, Chipika RH, Hardiman O, Bede P. The imaging signature of C9orf72 hexanucleotide repeat expansions: implications for clinical trials and therapy development. Brain Imaging Behav. 2021;15(5):2693-2719. doi:10.1007/s11682-020-00429-w
13. Westeneng HJ, Walhout R, Straathof M, et al. Widespread structural brain involvement in ALS is not limited to the C9orf72 repeat expansion. J Neurol Neurosurg Psychiatry. 2016;87(12):1354-1360. doi:10.1136/jnnp-2016-313959
14. Bede P, Elamin M, Byrne S, et al. Basal ganglia involvement in amyotrophic lateral sclerosis. Neurology. 2013a;81(24):2107-2115. doi:10.1212/01.wnl.0000437313.80913.2c
15. Byrne S, Elamin M, Bede P, et al. Cognitive and clinical characteristics of patients with amyotrophic lateral sclerosis carrying a C9orf72 repeat expansion: a population-based cohort study. Lancet Neurol. 2012;11(3):232-240. doi:10.1016/S1474-4422(12)70014-5
16. Bede P, Bokde AL, Byrne S, et al. Multiparametric MRI study of ALS stratified for the C9orf72 genotype. Neurology. 2013b;81(4):361-369. doi:10.1212/WNL.0b013e31829c5eee
17. Lee SE, Khazenzon AM, Trujillo AJ, et al. Altered network connectivity in frontotemporal dementia with C9orf72 hexanucleotide repeat expansion. Brain. 2014;137(11):3047-3060. doi:10.1093/brain/awu248
18. Lee SE, Sias AC, Mandelli ML, et al. Network degeneration and dysfunction in presymptomatic C9ORF72 expansion carriers. Neuroimage Clin. 2017;14:286-297. doi:10.1016/j.nicl.2016.12.006
19. Rytty R, Nikkinen J, Suhonen N, et al. Functional MRI in patients with the C9ORF72 expansion associate frontotemporal dementia. Mol Biol. 2014;3(117):10-4172. doi:10.4172/2168-9547.1000117
20. Smallwood Shoukry RF, Clark MG, Floeter MK. Resting state functional connectivity is decreased globally across the C9orf72 mutation spectrum. Front Neurol. 2020;11:598474. doi:10.3389/fneur.2020.598474
21. Menke RA, Proudfoot M, Wuu J, et al. Increased functional connectivity common to symptomatic amyotrophic lateral sclerosis and those at genetic risk. J Neurol Neurosurg Psychiatry. 2016;87(6):580-588.
22. Waugh RE, Danielian LE, Shoukry RFS, Floeter MK. Longitudinal changes in network homogeneity in presymptomatic C9orf72 mutation carriers. Neurobiol Aging. 2021;99:1-10. doi:10.1016/j.neurobiolaging.2020.11.014
23. Premi E, Calhoun VD, Diano M, et al. The inner fluctuations of the brain in presymptomatic frontotemporal dementia: the chronnectome fingerprint. Neuroimage. 2019;189:645-654. doi:10.1016/j.neuroimage.2019.01.080
24. Traynor B, Codd MB, Corr B, Forde C, Frost E, Hardiman O. Amyotrophic lateral sclerosis mimic syndromes: a population-based study. Arch Neurol. 2000;57(1):109-113.
25. Nigri A, Umberto M, Stanziano M, et al. C9orf72 ALS mutation carriers show extensive cortical and subcortical damage compared to matched wild-type ALS patients. Neuroimage Clin. 2023;38:103400. doi:10.1016/j.nicl.2023.103400
26. Jafri MJ, Pearlson GD, Stevens M, Calhoun VD. A method for functional network connectivity among spatially independent resting-state components in schizophrenia. Neuroimage. 2008;39(4):1666-1681. doi:10.1016/j.neuroimage.2007.11.001
27. Brooks BR, Miller RG, Swash M, Munsat TL. El Escorial revisited: revised criteria for the diagnosis of amyotrophic lateral sclerosis. Amyotroph Lateral Scler Other Motor Neuron Disord. 2000;1(5):293-299. doi:10.1080/146608200300079536
28. Balendra R, Jones A, Jivraj N, et al. Estimating clinical stage of amyotrophic lateral sclerosis from the ALS functional rating scale. Amyotroph Lateral Scler Frontotemporal Degener. 2014;15(3–4):279-284. doi:10.3109/21678421.2014.897357
29. Virtanen P, Gommers R, Oliphant TE, et al. SciPy 1.0: fundamental algorithms for scientific computing in python. Nat Methods. 2020;17(3):261-272. doi:10.1038/s41592-019-0686-2
30. Fischl B. FreeSurfer. Neuroimage. 2012;62(2):774-781. doi:10.1016/j.neuroimage.2012.01.021
31. Whitfield-Gabrieli S, Nieto-Castanon A. Conn: a functional connectivity toolbox for correlated and anticorrelated brain networks. Brain Connect. 2012;2(3):125-141. doi:10.1089/brain.2012.0073
32. Ashburner J, Friston KJ. Unified segmentation. Neuroimage. 2005;26(3):839-851. doi:10.1016/j.neuroimage.2005.02.018
33. Chai XJ, Castañón AN, Öngür D, Whitfield-Gabrieli S. Anticorrelations in resting state networks without global signal regression. Neuroimage. 2012;59(2):1420-1428. doi:10.1016/j.neuroimage.2011.08.048
34. Behzadi Y, Restom K, Liau J, Liu TT. A component based noise correction method (CompCor) for BOLD and perfusion based fMRI. Neuroimage. 2007;37(1):90-101. doi:10.1016/j.neuroimage.2007.04.042
35. Nieto-Castanon A. Handbook of Functional Connectivity Magnetic Resonance Imaging Methods in CONN. Hilbert Press; 2020.
36. Esteban O, Birman D, Schaer M, Koyejo OO, Poldrack RA, Gorgolewski KJ. MRIQC: advancing the automatic prediction of image quality in MRI from unseen sites. PloS One. 2017;12:e0184661. doi:10.1371/journal.pone.0184661
37. Chiò A, Moglia C, Canosa A, et al. ALS phenotype is influenced by age, sex, and genetics: a population-based

study. Neurology. 2020;94(8):e802-e810. doi:10.1212/WNL.0000000000008869
38. Del Mauro G, Del Maschio N, Sulpizio S, Fedeli D, Perani D, Abutalebi J. Investigating sexual dimorphism in human brain structure by combining multiple indexes of brain morphology and source-based morphometry. Brain Struct Funct. 2022;227(1):11-21. doi:10.1007/s00429-021-02376-8
39. Trojsi F, Di Nardo F, Caiazzo G, et al. Between-sex variability of resting state functional brain networks in amyotrophic lateral sclerosis (ALS). J Neural Transm. 2021;128(12):1881-1897.
40. Rooney J, Fogh I, Westeneng HJ, et al. C9orf72 expansion differentially affects males with spinal onset amyotrophic lateral sclerosis. J Neurol Neurosurg Psychiatry. 2017;88(4):281. doi:10.1136/jnnp-2016-314093
41. Bullmore E, Sporns O. Complex brain networks: graph theoretical analysis of structural and functional systems. Nat Rev Neurosci. 2009;10(3):186-198. doi:10.1038/nrn2575
42. Fornito A, Zalesky A, Bullmore E. Fundamentals of Brain Network Analysis. Academic Press; 2016.
43. Rubinov M, Sporns O. Complex network measures of brain connectivity: uses and interpretations. Neuroimage. 2010;52(3):1059-1069. doi:10.1016/j.neuroimage.2009.10.003
44. Sporns O, Honey CJ. Small worlds inside big brains. Proc Natl Acad Sci USA. 2006;103(51):19219-19220. doi:10.1073/pnas.0609523103
45. Zalesky A, Fornito A, Bullmore ET. Network-based statistic: identifying differences in brain networks. Neuroimage. 2010;53(4):1197-1207. doi:10.1016/j.neuroimage.2010.06.041
46. Caverzasi E, Battistella G, Chu SA, et al. Gyrification abnormalities in presymptomatic c9orf72 expansion carriers. J Neurol Neurosurg Psychiatry. 2019;90(9):1005-1010.
47. Floeter MK, Bageac D, Danielian LE, Braun LE, Traynor BJ, Kwan JY. Longitudinal imaging in C9orf72 mutation carriers: relationship to phenotype. Neuroimage Clin. 2016;12:1035-1043. doi:10.1016/j.nicl.2016.10.014
48. van Veenhuijzen K, Westeneng HJ, Tan HH, et al. Longitudinal Effects of Asymptomatic C9orf72 Carriership on Brain Morphology. Annals of Neurology; 2022.
49. Raichle ME, MacLeod AM, Snyder AZ, Powers WJ, Gusnard DA, Shulman GL. A default mode of brain function. Proc Natl Acad Sci USA. 2001;98(2):676-682. doi:10.1073/pnas.98.2.676
50. Raichle ME. The brain's default mode network. Annu Rev Neurosci. 2015;38:433-447. doi:10.1146/annurev-neuro-071013-014030
51. Gratton C, Sun H, Petersen SE. Control networks and hubs. Psychophysiology. 2018;55(3):e13032.
52. Witt ST, van Ettinger-Veenstra H, Salo T, Riedel MC, Laird AR. What executive function network is that? An image-based meta-analysis of network labels. Brain Topogr. 2021;34(5):598-607.
53. Menon V. Large-scale brain networks and psychopathology: a unifying triple network model. Trends Cogn Sci. 2011;15(10):483-506.
54. Fedeli D, Del Maschio N, Del Mauro G, Defendenti F, Sulpizio S, Abutalebi J. Cingulate cortex morphology impacts on neurofunctional activity and behavioral performance in interference tasks. Sci Rep. 2022;12(1):13684. doi:10.1038/s41598-022-17557-6
55. Hung Y, Gaillard SL, Yarmak P, Arsalidou M. Dissociations of cognitive inhibition, response inhibition, and emotional interference: voxelwise ALE meta-analyses of fMRI studies. Hum Brain Mapp. 2018;39(10):4065-4082.
56. Zhang R, Geng X, Lee T. Large-scale functional neural network correlates of response inhibition: an fMRI meta-analysis. Brain Struct Funct. 2017;222(9):3973-3990.
57. McKenna MC, Tahedl M, Murad A, et al. White matter microstructure alterations in frontotemporal dementia: phenotype-associated signatures and single-subject interpretation. Brain Behav. 2022;12(2):e2500. doi:10.1016/j.jns.2022.120221
58. Vatsavayai SC, Yoon SJ, Gardner RC, et al. Timing and significance of pathological features in C9orf72 expansion-associated frontotemporal dementia. Brain. 2016;139(12):3202-3216. doi:10.1093/brain/aww250
59. Arcaro MJ, Pinsk MA, Kastner S. The anatomical and functional organization of the human visual pulvinar. J Neurosci. 2015;35(27):9848-9871. doi:10.1523/JNEUROSCI.1575-14.2015
60. Bridge H, Leopold DA, Bourne JA. Adaptive pulvinar circuitry supports visual cognition. Trends Cogn Sci. 2016;20(2):146-157. doi:10.1016/j.tics.2015.10.003
61. Schmidt R, Verstraete E, de Reus MA, Veldink JH, van den Berg LH, van den Heuvel MP. Correlation between structural and functional connectivity impairment in amyotrophic lateral sclerosis. Hum Brain Mapp. 2014;35(9):4386-4395. doi:10.1002/hbm.22481
62. Hillary FG, Rajtmajer SM, Roman CA, et al. The rich get richer: brain injury elicits hyperconnectivity in core subnetworks. PloS One. 2014;9(8):e104021. doi:10.1371/journal.pone.0104021
63. Hillary FG, Roman CA, Venkatesan U, Rajtmajer SM, Bajo R, Castellanos ND. Hyperconnectivity is a fundamental response to neurological disruption. Neuropsychology. 2015;29(1):59-75. doi:10.1037/neu0000110
64. Hillary FG, Grafman JH. Injured brains and adaptive networks: the benefits and costs of hyperconnectivity. Trends Cogn Sci. 2017;21(5):385-401. doi:10.1016/j.tics.2017.03.003
65. Bullmore E, Sporns O. The economy of brain network organization. Nat Rev Neurosci. 2012;13(5):336-349. doi:10.1038/nrn3214

66. Mohammadi B, Kollewe K, Samii A, Krampfl K, Dengler R, Münte TF. Changes of resting state brain networks in amyotrophic lateral sclerosis. Exp Neurol. 2009;217 (1):147-153. doi:10.1016/j.expneurol.2009.01.025
67. Rittman T, Borchert R, Jones S, et al. Functional network resilience to pathology in presymptomatic genetic frontotemporal dementia. Neurobiol Aging. 2019;77:169-177.

Supporting Information

Additional supporting information may be found online in the Supporting Information section at the end of the article.

Table S1. Graph theoretical results (C9orf72+>ALSm), at different K cost thresholds.

